Blazars as a potential origin of the KM3-230213A event

Journal of Cosmology and Astroparticle Physics
An IOP and SISSA journal

Received: *November 19, 2025*
Revised: *January 15, 2026*
Accepted: *January 31, 2026*
Published: *March 11, 2026*

Blazars as a potential origin of the KM3-230213A event

The KM3NeT collaboration

Full author list at the end of the paper

E-mail: spokesperson@km3net.de, antonio.ambrosone@unina.it, meriem.bendahman@na.infn.it

Abstract: The KM3NeT collaboration has reported the detection of the highest energy neutrino event observed to date. The energy of the event is of the order of 220 PeV hinting towards a neutrino flux at the highest energies. In this article, the potential blazar origin for this event is explored. The publicly available Astro-Multimessenger Modeling software is used to model the blazar gamma-ray and neutrino fluxes. It is concluded that a population of blazars could produce the diffuse flux compatible with the observation of the ultra-high energy event detected by the KM3NeT/ARCA detector. At the same time, the gamma-ray flux produced by such a population of blazars is consistent with the diffuse gamma-ray flux measured by the Fermi Large Area Telescope.

Keywords: active galactic nuclei, neutrino astronomy, neutrino detectors, ultra high energy photons and neutrinos

ArXiv ePrint: 2511.13886

https://doi.org/10.1088/1475-7516/2026/03/033

JCAP03(2026)033

Contents

JCAP03(2026)033

1 Introduction

The KM3NeT collaboration is constructing two deep-sea neutrino detectors in the Mediterranean Sea: ARCA, optimised for the detection of high-energy cosmic neutrinos, offshore Sicily at a depth of about 3500 meters, and ORCA, off the coast of Toulon at about 2500 meters depth, dedicated to neutrino oscillation studies. Both detectors consist of vertical detection units equipped with optical modules housing photomultiplier tubes [1, 2]. Although still under construction, both detectors are already operational and delivering first results, demonstrating their potential in the area of multi-messenger astrophysics.

On February 13, 2023, an ultra-high energy neutrino event was observed by the KM3NeT/ARCA detector, which was operating with 21 detection units. The event represents the most energetic neutrino detected to date, with a reconstructed energy of 220^{+570}_{-110} PeV [3], which likely has an astrophysical origin. Soon after the publication of the discovery, several hypotheses have been suggested to interpret this event in an astrophysical framework. The possibility that the event is the signature of cosmogenic neutrinos has been explored in ref. [4], high-energy neutrinos produced in the interaction of Ultra-High Energy Cosmic Rays (UHECRs) with the photons from the extragalactic background light and the cosmic microwave background. Although cosmogenic neutrinos are guaranteed given the UHECR spectra measured by the Pierre Auger [5] and the Telescope Array [6] observatories, the large neutrino flux needed to account for KM3-230213A would imply that UHECRs should be injected up to very high redshift ($z \simeq 6$) with a subdominant proton component at the highest energies [4]. The possibility that the event is due to a powerful Galactic accelerator is discussed in ref. [7]. However, the lack of a gamma-ray counterpart as well as the need for this cosmic-ray accelerator to reach energies up to $\sim 4 \cdot 10^{18}$ eV make this hypothesis very unlikely. The possibility that the event might be produced by a single point-source is studied in ref. [8].

Several blazars, Active Galactic Nuclei (AGNi) with relativistic jets oriented towards the Earth, are consistent with the position of the event [9]. However, at present, the event is not associated with a specific source. Nonetheless, blazars remain well-motivated astrophysical sources (see [10] for a review). The IceCube Neutrino Observatory has found a correlation of $\sim 3\sigma$ for high-energy neutrino emission with a blazar named TXS 0506+056 [11, 12] confirming that blazar jets are accelerators of cosmic rays up to at least $\sim 1-10\,\mathrm{PeV}$ energies. Also, the ANTARES collaboration reported a $\sim 2\sigma$ hint of correlation between neutrino events and radio flaring blazars [13]. Furthermore, recent phenomenological analyses [14] have shown that blazars might emit neutrinos in the energy range between $\sim 1-100\,\mathrm{PeV}$.

In this article, the possibility that blazars accelerate cosmic rays along their jet axis and emit ultra-high energy neutrinos is studied. The complexity of blazar emissions is discussed under the most conservative astrophysical assumptions, so that the conclusions of this study are not influenced by model-specific details. High-energy gamma-ray and neutrino emissions from blazars are modelled using the publicly available Astro-Multimessenger Modeling (AM3) software [15]. This code implements a generic one-zone model for the relativistic jets and incorporates particle acceleration and emission processes, including both leptonic and hadronic interactions. A statistical analysis is performed to probe the parameter space and investigate under which condition blazars might have produced the event. In this regard, any diffuse flux interpretation of the event must be compatible with the diffuse gamma-ray measurements from the Fermi Large Area Telescope (Fermi-LAT) and the lack of a counterpart from other neutrino telescopes such as IceCube and Auger [16–20]. This analysis shows that a blazar population is consistent with observational constraints and can produce the required flux for KM3-230213A.

The article is organised as follows: the single blazar geometrical setup and the model assumptions for the simulation of the neutrino and gamma-ray emissions are described in section 2. The diffuse flux calculation is discussed in section 3, while sections 4 and 5 describe how effective areas are evaluated and datasets statistically processed. The results and the impact of systematic uncertainties are reported in section 6. Section 7 summarises the results of the work. Finally, a statistical analysis using KM3NeT/ARCA-only information to show that the result is compatible with the gamma-ray constraints imposed by the Fermi-LAT collaboration is presented in appendix A.

2 Blazar simulation: source model and assumptions

In this section, details of the simulation of high-energy neutrino emitters from a single blazar are discussed. The AM3 software, which solves time-dependent transport equations for primary and secondary particles in astrophysical jets, is used to predict multi-messenger emissions. It implements a single-zone model where the emission region is treated as a compact spherical blob moving with relativistic velocity along the jet. The jet is modelled as a relativistic outflow with a bulk Lorentz factor Γ_b fixed at 17.6, the mean value obtained by [21] (also adopted as the default in the AM3 software [15]), which defines the jet speed relative to the observer. Following [21], the jet is assumed to be observed at small angle $\theta_{\mathrm{obs}} \lesssim \frac{1}{\Gamma_b}$ relative to its axis, leading to a Doppler boosting factor $\delta_D = \Gamma_b$.

JCAP03(2026)033

$\log_{10}(R')$ [cm]	Γ_b	B' [G]	$\log_{10}(R_{\rm diss})$ [cm]	$\frac{R_{\rm diss}}{R_{\rm BLR}}$	$\log_{10}(\Gamma_{\rm e\ max})$	$\log_{10}(\Gamma_{\rm p\ max})$	α_e	$\log_{10}(L_{\rm e})$ [erg/s]
15.9	17.6	2.6	16.8	1.8	4.7	7.5	1.7	41.2

Table 1. Fixed source parameters used in the AM3 simulation. Values correspond to the average reported in [14].

The particle acceleration is described by a power-law with spectral indices α_p and α_e for protons and electrons, respectively. In the following analysis, the maximum electron and proton energies, in the jet reference frame, are fixed at 25 GeV and 30 PeV, respectively. These values are consistent with the average value determined by using a catalogue of 32 blazars [14]. Larger values of the maximum proton energy do not affect the conclusions of this article, while smaller ones would prevent blazars from producing neutrinos energetic enough to explain KM3-230213A.

The other parameters defined in the AM3 simulations are:

- Radius ($R^{'}$): characteristic size of the blazar's emission region.
- Magnetic Field (B'): strength of the magnetic field within the jet.
- $R_{\rm BLR}$: the radius of the Broad Line Region, fast-moving gas clouds responsible for broad optical and UV lines.
- $R_{\rm diss}$: dissipation radius in the jet, relative to $\rm R_{BLR}$ controlling external photon impact.
- $\Gamma_{\rm e\ max}$: maximum Lorentz factor for electrons.
- $\Gamma_{\rm p\ max}$: maximum Lorentz factor for protons.
- Electron Luminosity (L_e): luminosity associated with the relativistic electrons in the jet.
- Proton Luminosity (L_p): luminosity associated with the relativistic protons in the jet.
- Baryonic Loading ($\eta = L_p/L_e$): this parameter characterises the ratio of proton to electron luminosity.

Since it is not feasible to account for the variability of each parameter across the whole blazar population, some of the above-mentioned parameters are fixed at the average values reported in [14], which are consistent with the parameter ranges derived from the catalogue of 324 nearby blazars in [21]. These values are summarised in table 1 and define the baseline AM3 source template.

In the following, the baryonic loading (η), and the proton spectral index (α_p) are treated as free parameters. The baryonic loading modifies the normalisation of the gamma-ray and neutrino spectra while the spectral index determines their shape. These two parameters effectively capture the full variability of these spectra among the sources.

The AM3 software implements all the main processes for the production of secondary particles. They are summarised in the following.

JCAP03(2026)033

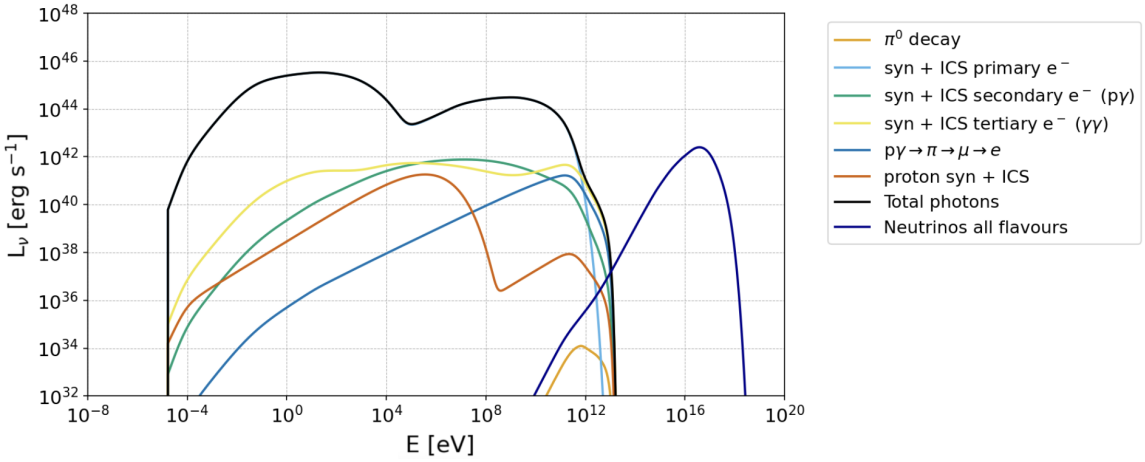

Figure 1. Differential luminosity for gamma-rays and neutrinos (all-flavour) as a function of the energy. The values of the baryonic loading and the proton spectral index have been fixed at 10 and 1.8, respectively.

- Synchrotron radiation: electrons accelerated in the jet produce synchrotron radiation.
- Inverse Compton Scattering (ICS): both synchrotron self-Compton and external Compton scattering contribute to the observed high-energy radiation from the jet: $e^- + \gamma \to e^- + \gamma$.
- Bethe-Heitler Pair Production: protons interacting with photons in the jet produce electron-positron pairs: $p + \gamma \to p + e^+ + e^-$.
- Pair production: photon-photon interactions lead to the creation of electron-positron pairs: $\gamma + \gamma \to e^+ + e^-$.
- Pion Decay from photomeson interactions: high-energy protons in the jet interact with ambient photons, producing pions that decay into gamma-rays and neutrinos:

$$p + \gamma \to \begin{cases} p + \pi^0 \\ n + \pi^+ \end{cases} \to \begin{cases} 2\gamma + X \\ \nu_\mu + e^+ + \nu_e + \bar{\nu}_\mu + X \end{cases} .$$

Modelling these processes using AM3 allows for the computation of the differential photon flux and the differential neutrino flux from a single simulated blazar. A benchmark case of the luminosity (in unit of erg s^{-1}) is shown in figure 1 for a single blazar as a function of the energy, using $\eta = 10$ and $\alpha_p = 1.8$ (these values correspond to the best-fit values found by this analysis, see below for more details). For completeness, the different processes are shown separately to evaluate their individual contribution to the overall gamma-ray spectrum and to the overall neutrino spectrum. The low-energy cutoff comes from the energy range adopted for the simulations.

JCAP03(2026)033

3 Diffuse flux calculation

The blazar diffuse flux is calculated through the gamma-ray luminosity function, following [22]. The luminosity function at $z = 0$ is defined as:

$$\mathcal{S}(L_\gamma, z = 0, \Gamma) = \frac{dN}{dL_\gamma \, dV_c \, d\Gamma} = \frac{A}{\ln(10) \, L_\gamma} \left(\left(\frac{L_\gamma}{L_*} \right)^{\gamma_1} + \left(\frac{L_\gamma}{L_*} \right)^{\gamma_2} \right)^{-1} \times e^{-0.5 \frac{[\Gamma_{\rm ph} - \mu(L_\gamma)]^2}{\sigma^2}}, \tag{3.1}$$

where L_γ is the $0.1 - 100\,\mathrm{GeV}$ rest-frame gamma-ray integrated luminosity in units of $\mathrm{GeV\,s^{-1}}$ and V_c is the comoving volume. $\Gamma_{\rm ph}$ represents the photon flux index that follows a Gaussian distribution, with μ and σ denoting the mean and dispersion of the distribution, respectively. μ is expressed in terms of L_γ as:

$$\mu(L_\gamma) = \mu_* + \beta \times \Big[\log_{10}(L_\gamma) - 46 \Big]. \tag{3.2}$$

The luminosity function at a given redshift z is then given by:

$$\mathcal{S}(L_\gamma, z, \Gamma) = \mathcal{S}(L_\gamma, z = 0, \Gamma) \times e(z, L_\gamma), \tag{3.3}$$

where

$$e(z, L_\gamma) = (1 + z)^{k_d(L_\gamma)} e^{\frac{z}{\zeta}}, \tag{3.4}$$

with $k_d(L_\gamma) = k_* + \tau_\gamma(\log_{10}(\mathrm{L}_\gamma) - 46)$.

All the numerical values of the parameters $(A, L_*, \gamma_1, \gamma_2, k_*, \zeta, \tau_\gamma, \mu_*, \beta, \sigma)$ are reported in table 2. Since in the model used in this analysis there is no $\Gamma_{\rm ph}$ parameter, the final luminosity function $\mathcal{S}(L_\gamma, z)$ is given by

$$\mathcal{S}(L_\gamma, z) = \int_1^{3.5} d\Gamma_{\rm ph} \, \mathcal{S}(L_\gamma, z, \Gamma_{\rm ph}). \tag{3.5}$$

This is the same approach used in ref. [23]. The diffuse blazar flux is calculated with

$$\begin{aligned} \Phi^{\nu,\gamma}_{\rm Diff}(E, \eta, \alpha_p) = & \int_{10^{-3}}^{6} dz \int_{10^{43}\,\mathrm{erg\,s^{-1}}}^{10^{52}\,\mathrm{erg\,s^{-1}}} dL_\gamma \, \mathcal{S}(L_\gamma, z) \\ & \times \frac{dN}{dE \, dA \, dt}(E, \eta, \alpha_p, L_\gamma, z) \, e^{-\tau^{\nu,\gamma}(E,z)} \, \frac{dV_c}{dz}(z) \,, \end{aligned} \tag{3.6}$$

where $\frac{dN}{dEdAdt}(E, \eta, \alpha_p, L_\gamma, z)$ describes the single blazar gamma-ray and neutrino spectra from AM3 including the correction for energy redshift. $\frac{dV_c}{dz}(z)$ represents the Jacobian of the transformation from V_c to z. $\tau^\nu(E, z)$ is the neutrino optical depth equal to zero because they propagate unimpeded, and $\tau^\gamma(E, z)$ is the gamma-ray optical depth which is implemented following ref. [24].

4 Effective areas

Figure 2 reports the comparison between the effective areas $(A_{\rm eff}(E))$ between the KM3NeT/ARCA and the IceCube detectors in terms of the neutrino energy. $A_{\rm eff}(E)$ are reported for all-flavours averaged between neutrinos and anti-neutrinos. Furthermore, they are averaged over the whole sky.

JCAP03(2026)033

A [Gpc^{-3}]	$\log_{10}(L_*)$ [erg s^{-1}]	γ_1	γ_2	k_*	ζ	τ_γ	μ_*	β	σ
$1.22 \cdot 10^{-2}$	47.64	2.80	1.26	12.14	-0.15	2.79	2.22	0.10	0.28

Table 2. Values of the parameters for the luminosity distribution function [22].

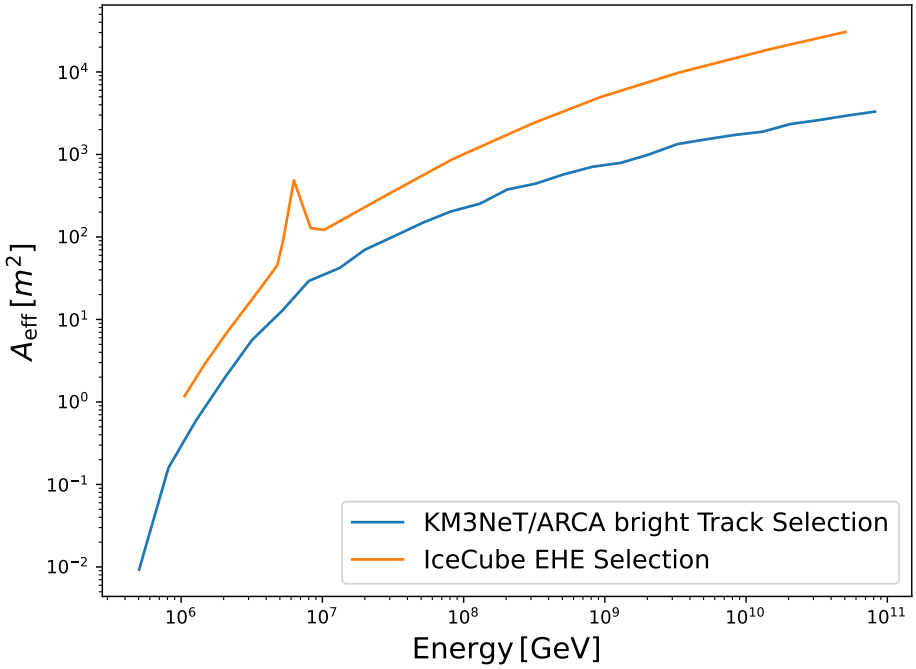

Figure 2. Comparison between the KM3NeT/ARCA with a configuration of 21 detection lines [3] and IceCube [17] effective areas in terms of energy. The effective areas are summed over all-flavours and averaged between neutrinos and anti-neutrinos.

Figure 2 shows the KM3NeT/ARCA effective area calculated for the detector configuration comprising 21 detection lines, corresponding to the setup at the time of the event discovery. Only track-like events are considered, hereafter referred to simply as *tracks*, i.e. events involving the production of a muon traversing the detector and emitting Cherenkov light. In particular, the *bright track* selection described in ref. [3] is used. This selection requires a minimum number of triggered photomultipliers, $N_{\text{trig}}^{\text{PMT}} \geq 1500$, a reconstructed track length $L_{\text{track}} \geq 250\,\text{m}$, and a track-reconstruction log-likelihood ratio exceeding 500. This selection ensures that only good quality events with a brightness comparable to that of the KM3-230213A event are included in the calculation of the expected number of signal events.

For the IceCube detector, the effective area reported in ref. [17] is adopted. This effective area is derived using the extreme high-energy (EHE) event selection, which involves cuts on the total deposited charge and the number of hits, and on the quality of the reconstructed tracks, with an additional background suppression provided by the IceTop veto. Both event selections are characterized by an extremely low expected background rate, which is neglected in the following analysis. For both detectors, the effective areas are dominated by horizontal

JCAP03(2026)033

and downgoing events, since upgoing events are significantly attenuated by the Earth at energies $E \gtrsim 10\,\mathrm{PeV}$. The total exposure is defined as

$$\epsilon_{\mathrm{eff}}^{\mathrm{tot}}(E) = 4\pi \left[T_{\mathrm{KM3}}\, A_{\mathrm{eff}}^{\mathrm{KM3}}(E) + T_{\mathrm{IC}}\, A_{\mathrm{eff}}^{\mathrm{IC}}(E) \right], \tag{4.1}$$

where $T_{\mathrm{KM3}} = 335\,\mathrm{days}$ and $T_{\mathrm{IC}} = 12.6\,\mathrm{yr}$ denote the KM3NeT and IceCube detector live times, respectively.

5 Likelihood analysis

In order to interpret the KM3-230213A event in terms of a diffuse neutrino flux from blazars, the following constraints must be satisfied:

- the diffuse neutrino flux from blazars should be compatible with the non-observation of high-energy neutrino events reported by the IceCube and Auger collaborations;
- the diffuse gamma-ray flux from blazars cannot be larger than the extragalactic background gamma-ray flux measured by the Fermi-LAT collaboration, also known as the EGB spectrum [16].

For the neutrino part, the likelihood function describing the neutrino emission is defined as the Poisson probability of observing $n_s = 1$ event with an expected number of events given by $\lambda^{\mathrm{tot}}(\eta, \alpha_p)$

$$\mathcal{L}_\nu(\eta, \alpha_p) = \lambda^{\mathrm{tot}}(\eta, \alpha_p) e^{-\lambda^{\mathrm{tot}}(\eta, \alpha_p)}, \tag{5.1}$$

where $\lambda^{\mathrm{tot}}(\eta, \alpha_p)$ is estimated as

$$\lambda^{\mathrm{tot}}(\eta, \alpha_p) = \int_{\Delta E} \epsilon_{\mathrm{eff}}^{\mathrm{tot}}(E) \Phi_{\mathrm{Diff}}^{\nu}(E, \eta, \alpha_p) dE, \tag{5.2}$$

where $\epsilon_{\mathrm{eff}}^{\mathrm{tot}}(E)$ is the total exposure introduced in the previous section. As in [25], measurements from both detectors are combined for energies above 10 PeV. In this work, the exposure of Pierre Auger [18] is not included, because IceCube currently provides higher sensitivity in the energy range where blazars are assumed to emit neutrinos. In order to suppress the parameters producing a diffuse gamma-ray flux overshooting the Fermi-LAT measurements, a Gaussian penalty term is introduced in the likelihood function as in ref. [26]:

$$\mathcal{L}_\gamma(\eta, \alpha_p) = e^{-\frac{1}{2}\left(\frac{f(\eta, \alpha_p) - 0.86}{0.14}\right)^2}, \tag{5.3}$$

where f represents the integrated fraction of the diffuse gamma-ray spectrum between $50 - 2000\,\mathrm{GeV}$:

$$f(\eta, \alpha_p) = \frac{\int_{50\,\mathrm{GeV}}^{2000\,\mathrm{GeV}} dE\, \Phi_{\mathrm{diff}}^{\gamma}(E, \eta, \alpha_p)}{F_{\mathrm{Fermi-LAT}}^{\gamma}}, \tag{5.4}$$

and $F_{\mathrm{Fermi-LAT}}^{\gamma} = 2.4 \cdot 10^{-9} \mathrm{photon\,cm^{-2}\,s^{-1}\,sr^{-1}}$ is the total diffuse flux measured by the Fermi-LAT telescope [27]. This fraction has been estimated in ref. [27] to be $(86\%^{+16\%}_{-14\%})$. Although the value ascribed to blazars is subject to significant uncertainties due to specific

JCAP03(2026)033

assumptions [28], in this analysis this fraction is used solely to avoid exceeding the Fermi-LAT measurements. Therefore, this uncertainty does not affect the final conclusions of the present work. The total likelihood of the model is the product of the photon and neutrino likelihood functions:

$$\mathcal{L}_{\rm tot}(\eta, \alpha_p) = \mathcal{L}_\nu(\eta, \alpha_p)\mathcal{L}_\gamma(\eta, \alpha_p). \tag{5.5}$$

The parameter space is explored using the test statistic (TS) defined as:

$$\mathrm{TS}(\eta, \alpha_{\rm p}) = 2 \cdot \ln\left(\frac{\mathcal{L}_{\rm tot}(\tilde{\eta}, \tilde{\alpha_{\rm p}})}{\mathcal{L}_{\rm tot}(\eta, \alpha_{\rm p})}\right), \tag{5.6}$$

where $\tilde{\eta}$ and $\tilde{\alpha_p}$ are the parameters that maximise the overall likelihood. According to Wilks' theorem [29], the test statistic follows a chi-squared distribution with 2 degrees of freedom, as the number of free parameters.

6 Results and discussion

The $1, 2, 3\,\sigma$ TS contours are shown in figure 3. The best fit indicates values of $\tilde{\eta} \approx 10$ and $\tilde{\alpha_p} \approx 1.8$. The result also suggests that η values larger than 100 are strongly disfavoured above the 3σ level. Furthermore, the analysis favours hard spectral indices, $\alpha_p \lesssim 2$, which maximise the expected number of events in KM3NeT/ARCA and IceCube within the considered energy range ΔE.

The statistical analysis is dominated by the neutrino contribution to the likelihood (eq. (5.1)) and yields a predicted neutrino spectrum, shown in figure 4, which closely matches the joint E^{-2} fit reported in ref. [25]. The 1σ band for the blazar diffuse flux is compatible with the differential upper limits reported by IceCube [17] and Auger [19]. The spectrum is also consistent with the diffuse neutrino flux upper limits derived from other IceCube data samples [31–33] and from the ANTARES collaboration [34]. In this scenario, blazars contribute negligibly to the diffuse neutrino flux at energies $\lesssim 1\,\mathrm{PeV}$. The corresponding gamma-ray spectrum is compatible with the 2FGL resolved source catalogue [16], with blazars contributing $\simeq 42\%$ of the EGB as shown in figure 5. Although this value is lower than the 86% fraction adopted in eq. (5.3), this does not indicate any tension with the gamma-ray flux. In fact, the total diffuse gamma-ray flux is dominated by leptonic contributions (see figure 1), and this analysis cannot constrain all the parameters listed in table 1, such as the electron luminosity. Therefore, the adopted blazar fraction (eq. (5.4)) is regarded as an upper limit to avoid overproducing gamma rays.

It is also verified that variations of a factor ~ 2 in the benchmark values reported in table 1 for the magnetic field (B), the radius (R'), and the electron spectral index (α_e) affect the diffuse flux calculation at the $\lesssim 5\%$ level; therefore, source-to-source variations do not significantly alter the conclusions of this analysis.

This suggests that blazars may contribute significantly to the UHE neutrino emission leading to KM3-230213A. Notably, even when considering only KM3NeT data (see appendix A for details), the inferred diffuse neutrino spectrum remains consistent with EGB measurements. In this case, the most stringent constraints arise from diffuse neutrino observations in the

JCAP03(2026)033

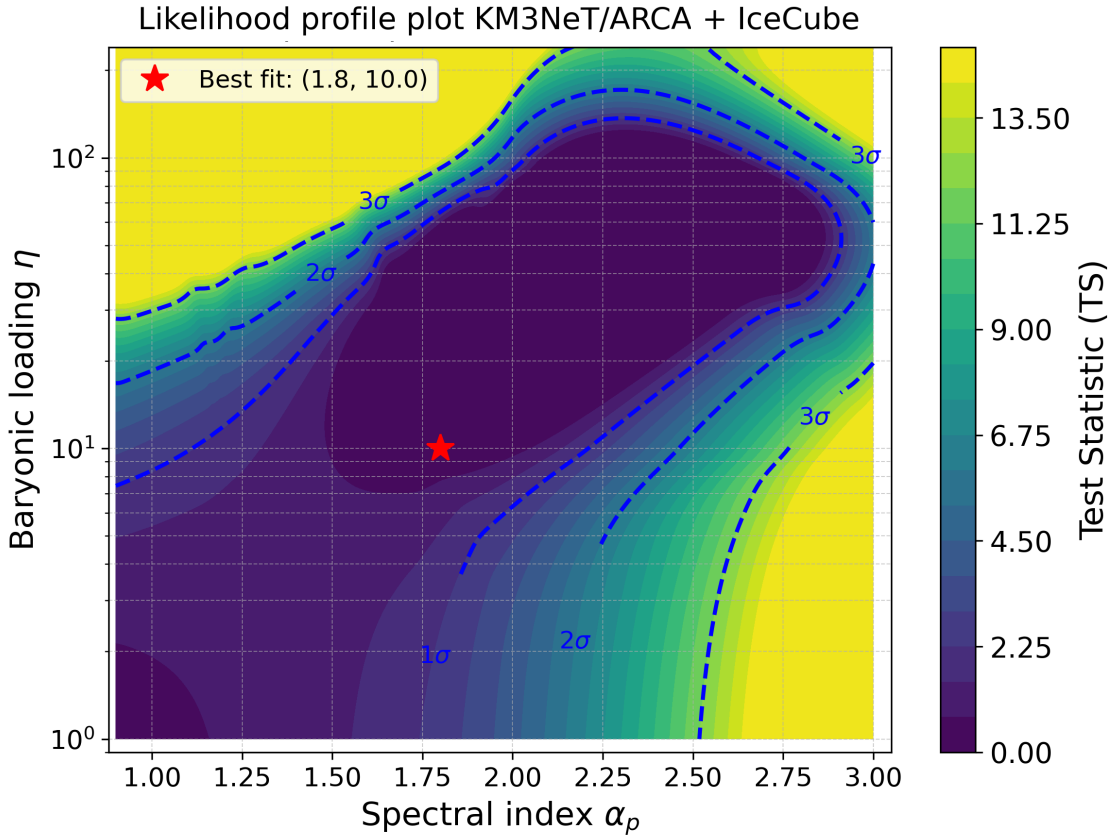

Figure 3. Test statistic contour plot in terms of baryonic loading (η) and the proton spectral index (α_p) for the joint KM3NeT/ARCA and IceCube analysis. The best-fit value is reported with a red star.

$\sim$ 1–10 PeV range, where blazars nearly saturate the upper limits. To explain such a high neutrino flux, blazars would need to be approximately a hundred times more luminous, corresponding to baryonic loadings $\eta \simeq 10^3$.

Impact of systematic uncertainties. The analysis presented already exploits the information provided by the observation of a single extreme event, and is driven by the statistical uncertainty on the neutrino flux derived from an unique observation. Consequently, the dominant sources of systematic uncertainty are associated with the determination of the detectors effective areas. Uncertainties in the effective areas arise primarily from the response of the digital optical modules to incident photons, as well as from the absorption and scattering properties of the propagation medium, namely water for KM3NeT and ice for IceCube. These effects lead to an overall uncertainty on the effective areas estimated to be at the level of $\sim$ 10%, as reported in ref. [35]. An additional contribution originates from the uncertainty on the neutrino interaction cross section, which is known with a precision of approximately 20% at energies above 10^4 GeV [17]. Combining these contributions conservatively, the total systematic uncertainty affecting the results presented in this manuscript is estimated to be at

JCAP03(2026)033

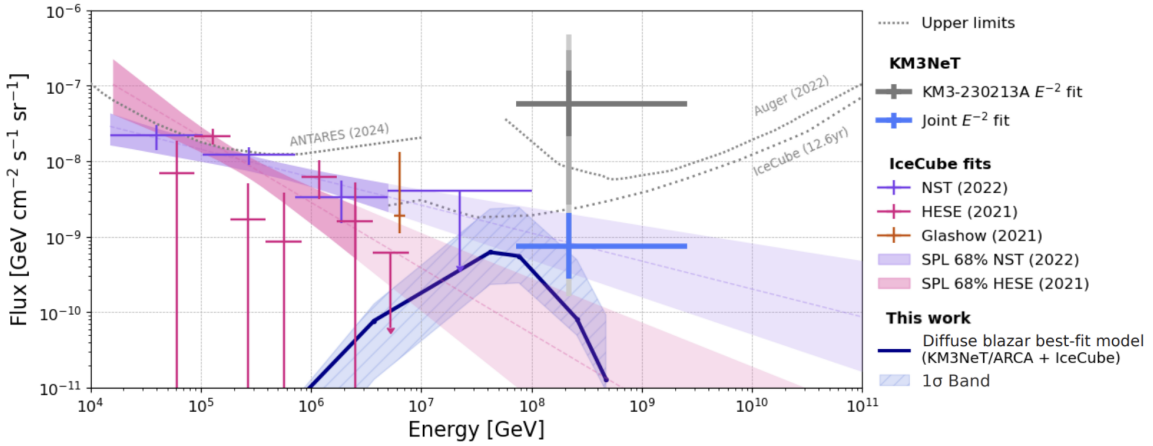

Figure 4. Neutrino diffuse spectral energy distribution for blazars in terms of the energy for a single neutrino flavour. The dark blue solid line represents the best fit, while the shaded region is the 1σ band. The prediction is compared with the KM3-230213A equivalent flux [3], the joint E^{-2} flux obtained by [25] including IceCube-Extreme High-Energy [30] and Auger non-observations, and the updated IceCube [17] and Auger differential upper limits [19]. For comparison, the diffuse neutrino flux measured by the IceCube Neutrino Observatory with several samples [31–33] and also the ANTARES upper limits [34] are reported. The pink and purple shaded regions represent the IceCube single-power-law (SPL) fits for High-Energy Starting Events (HESE) [31] and Northern Sky Tracks (NST) [32], respectively.

the level of $\sim 30\%$, therefore subdominant with respect to the statistical uncertainty. Such an uncertainty does not alter the main conclusions of the analysis.

7 Conclusions

The KM3NeT collaboration has reported the highest-energy neutrino event detected to date, with an estimated energy of $\sim 220\,\mathrm{PeV}$. In this article, the possibility that this event might have originated from the diffuse neutrino flux produced by blazars is considered. This is theoretically well motivated since blazars are the most luminous objects in the gamma-ray sky. In order to constrain the spectrum of a single blazar, the publicly available AM3 software is used. In order to extrapolate this result to the whole blazar population, the luminosity function inferred by the Fermi-LAT collaboration is used. The constraints imposed by the IceCube non-observation and the gamma-ray measurements from Fermi-LAT are also taken into account. Results demonstrate that the diffuse neutrino flux due to blazars is compatible with all constraints and may explain the KM3-230213A event considering a joint fit combining information with the IceCube diffuse flux measurement. In appendix A, the case of the KM3NeT/ARCA exposure alone is discussed. In this case, the diffuse emission from blazars remains consistent with Fermi-LAT gamma-ray constraints, though it is in tension with the IceCube upper limits at the ~ 2.5–$3\,\sigma$ level.

JCAP03(2026)033

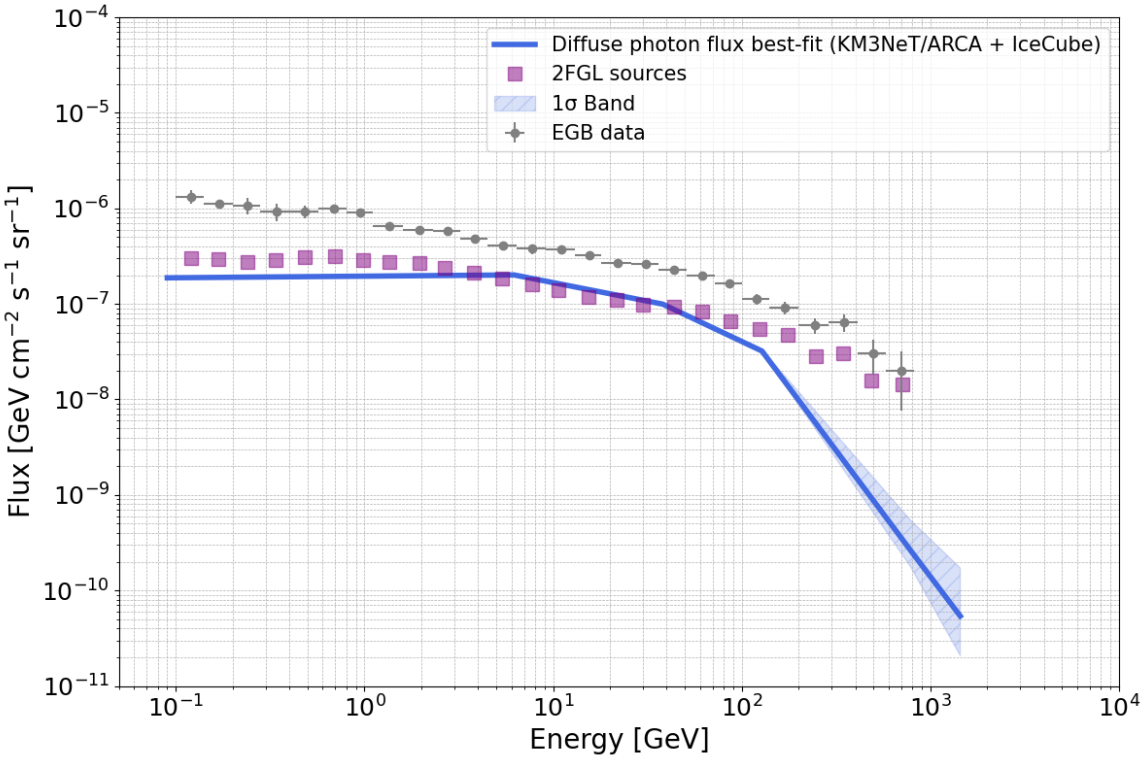

Figure 5. Gamma-ray diffuse spectral energy distribution for blazars as a function of the energy. The solid line represents the best fit while the shaded region the 1σ band. The result is compared with ExtraGalactic Background measurements of Fermi-LAT and the 2FGL sources [16].

Acknowledgments

The authors acknowledge the financial support of: KM3NeT-INFRADEV2 project, funded by the European Union Horizon Europe Research and Innovation Programme under grant agreement No 101079679; Funds for Scientific Research (FRS-FNRS), Francqui foundation, BAEF foundation. Czech Science Foundation (GAČR 24-12702S); Agence Nationale de la Recherche (contract ANR-15-CE31-0020), Centre National de la Recherche Scientifique (CNRS), Commission Européenne (FEDER fund and Marie Curie Program), LabEx UnivEarthS (ANR-10-LABX-0023 and ANR-18-IDEX-0001), Paris Île-de-France Region, Normandy Region (Alpha, Blue-waves and Neptune), France, The Provence-Alpes-Côte d'Azur Delegation for Research and Innovation (DRARI), the Provence-Alpes-Côte d'Azur region, the Bouches-du-Rhône Departmental Council, the Metropolis of Aix-Marseille Provence and the City of Marseille through the CPER 2021-2027 NEUMED project, The CNRS Institut National de Physique Nucléaire et de Physique des Particules (IN2P3); Shota Rustaveli National Science Foundation of Georgia (SRNSFG, FR-22-13708), Georgia; This research was funded by the European Union (ERC MuSES project No 101142396); The General Secretariat of Research and Innovation (GSRI), Greece; Istituto Nazionale di Fisica Nucleare (INFN) and Ministero dell'Università e della Ricerca (MUR), through PRIN 2022 program (Grant PANTHEON 2022E2J4RK, Next Generation EU) and PON R&I program (Avviso n. 424 del 28 febbraio 2018, Progetto PACK-PIR01 00021), Italy; IDMAR project Po-Fesr

JCAP03(2026)033

Sicilian Region az. 1.5.1; A. De Benedittis, W. Idrissi Ibnsalih, M. Bendahman, A. Nayerhoda, G. Papalashvili, I. C. Rea, A. Simonelli have been supported by the Italian Ministero dell'Università e della Ricerca (MUR), Progetto CIR01 00021 (Avviso n. 2595 del 24 dicembre 2019); KM3NeT4RR MUR Project National Recovery and Resilience Plan (NRRP), Mission 4 Component 2 Investment 3.1, Funded by the European Union — NextGenerationEU,CUP I57G21000040001, Concession Decree MUR No. n. Prot. 123 del 21/06/2022; Ministry of Higher Education, Scientific Research and Innovation, Morocco, and the Arab Fund for Economic and Social Development, Kuwait; Nederlandse organisatie voor Wetenschappelijk Onderzoek (NWO), the Netherlands; The grant "AstroCeNT: Particle Astrophysics Science and Technology Centre", carried out within the International Research Agendas programme of the Foundation for Polish Science financed by the European Union under the European Regional Development Fund; The program: "Excellence initiative-research university" for the AGH University in Krakow; The ARTIQ project: UMO-2021/01/2/ST6/00004 and ARTIQ/0004/2021; Ministry of Education and Scientific Research, Romania; Slovak Research and Development Agency under Contract No. APVV-22-0413; Ministry of Education, Research, Development and Youth of the Slovak Republic; MCIN for PID2021-124591NB-C41, -C42, -C43 and PDC2023-145913-I00 funded by MCIN/AEI/10.13039/501100011033 and by "ERDF A way of making Europe", for ASFAE/2022/014 and ASFAE/2022 /023 with funding from the EU NextGenerationEU (PRTR-C17.I01) and Generalitat Valenciana, for Grant AST22_6.2 with funding from Consejería de Universidad, Investigación e Innovación and Gobierno de España and European Union — NextGenerationEU, for CSIC-INFRA23013 and for CNS2023-144099, Generalitat Valenciana for CIDEGENT/2020/049, CIDEGENT/2021/23, CIDEIG/2023/20, ESGENT2024/24, CIPROM/2023/51, GRISOLIAP/2021/192 and INNVA1/2024/110 (IVACE+i), Spain; Khalifa University internal grants (ESIG-2023-008, RIG-2023-070 and RIG-2024-047), United Arab Emirates; The European Union's Horizon 2020 Research and Innovation Programme (ChETEC-INFRA — Project no. 101008324).

Views and opinions expressed are those of the author(s) only and do not necessarily reflect those of the European Union or the European Research Council. Neither the European Union nor the granting authority can be held responsible for them.

JCAP03(2026)033

A Likelihood analysis with only KM3NeT information

In this section, the results of the likelihood analysis are reported, considering only the KM3NeT/ARCA exposure in eq. (5.1).

The 1, 2 and 3 σ TS contours are shown in figure 6. In this case, the best-fit value is $\eta \approx 10^3$ and $\alpha_p \approx 1.75$. The best-fit spectral index is close to the value obtained when the IceCube exposure is included in the likelihood analysis. However, in this case the baryonic loading value maximizing the likelihood is ~ 2 orders of magnitude higher than for the joint analysis. The two results are compatible within about 2.5–3 σ.

The best fit and 1σ bands for neutrinos and photons are shown in figures 7 and 8, respectively, and are compared with the corresponding measurements discussed in the main text. The neutrino spectrum is compatible with the one reported by [3] although it is in tension with the IceCube measurements reported in the $\sim 100 - 1000$ TeV energy range. Furthermore, the flux is in tension with the Auger and IceCube upper limits at energies above ~ 100 PeV.

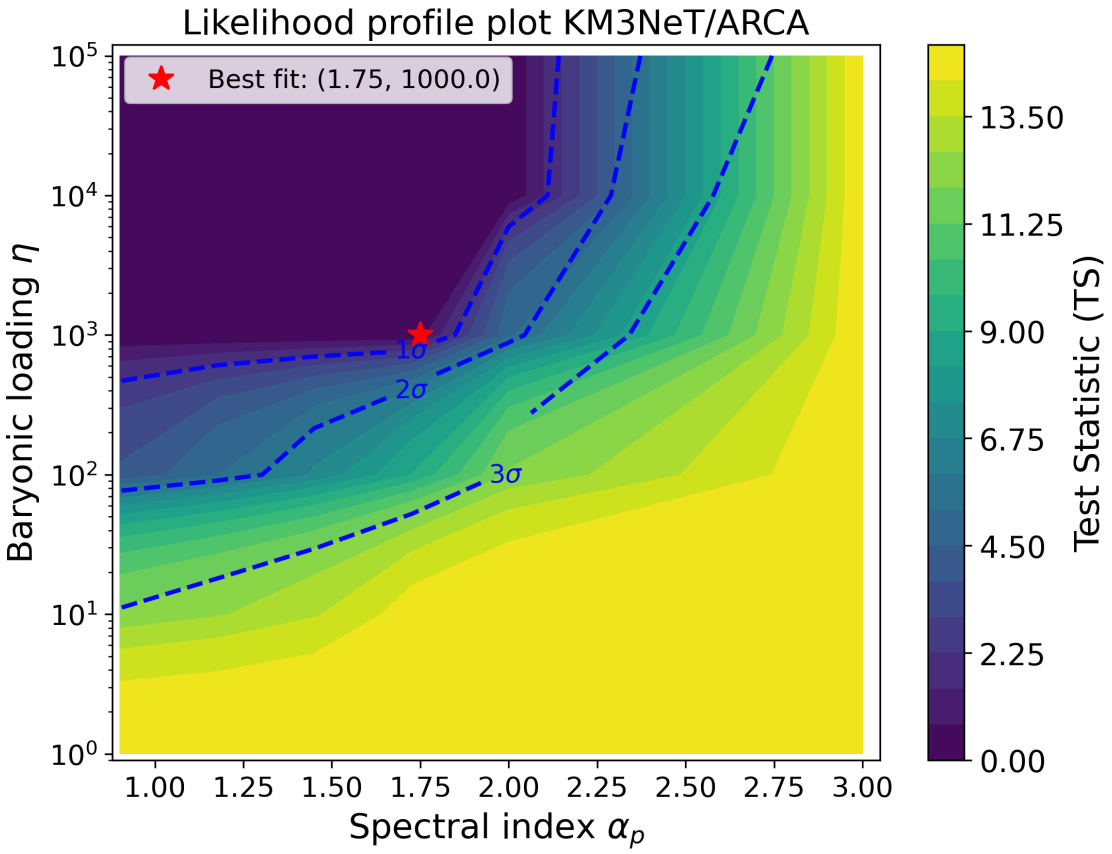

Figure 6. Test statistic contour plot in terms of baryonic loading (η) and the proton spectral index (α_p) for the KM3NeT/ARCA-only analysis. The best-fit value is reported with a red star.

This suggests that more luminous sources are required to enable the detection of ~ 1 event in KM3NeT/ARCA. However, the corresponding gamma-ray flux is consistent with Fermi-LAT constraints; in fact, the fraction produced by blazars is $\simeq 77\%$, as shown in figure 8.

JCAP03(2026)033

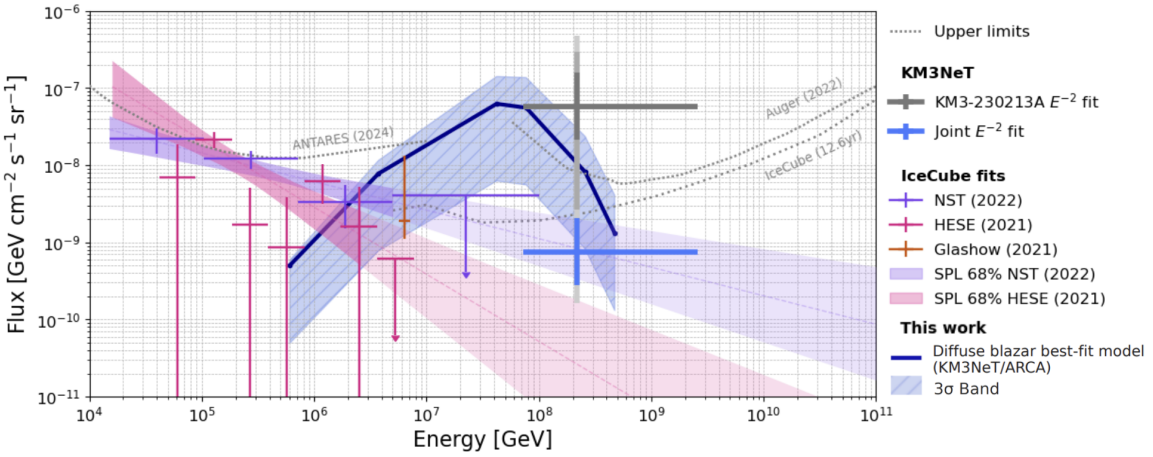

Figure 7. Neutrino diffuse spectral energy distribution for blazars in terms of the energy for a single neutrino flavour. The dark blue line represents the best fit while the shaded region is the 3σ band. The prediction is compared with the KM3-230213A equivalent flux [3], the joint E^{-2} flux obtained by [25] including IceCube-Extreme High-Energy [30] and Auger non-observations, and the updated IceCube [17] and Auger differential upper limits [19]. For comparison, the diffuse neutrino flux measured by the IceCube Neutrino Observatory with several samples [31–33]and also the ANTARES upper limits [34] are reported. The pink and purple shaded regions represent the IceCube single-power-law (SPL) fits for High-Energy Starting Events (HESE) [31] and Northern Sky Tracks (NST) [32], respectively.

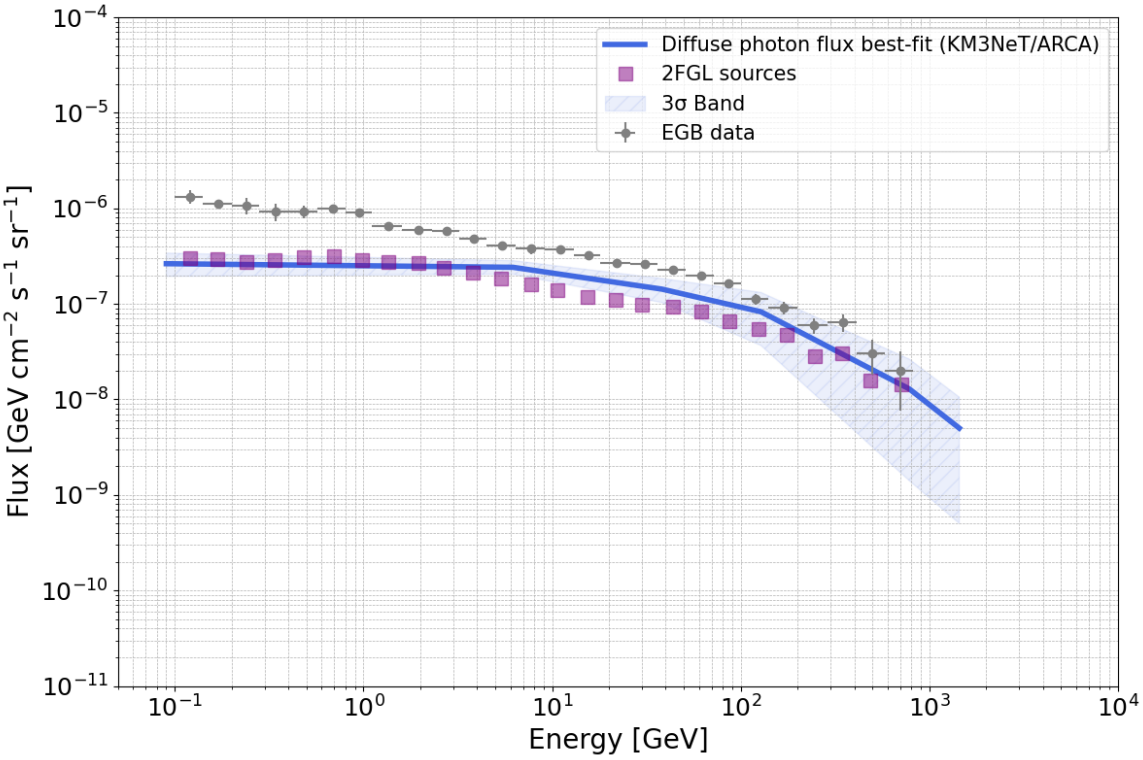

Figure 8. Gamma-ray diffuse spectral energy distribution for blazars as a function of the energy. The solid line represents the best fit while the shaded region represents the 3σ band. The result is compared with ExtraGalactic Background (EGB) measurements of Fermi-LAT and the 2FGL sources [16].

JCAP03(2026)033

References

[1] KM3NeT collaboration, *The KM3NeT multi-PMT optical module*, 2022 *JINST* **17** P07038 [arXiv:2203.10048] [INSPIRE].

[2] S. Aiello et al., *Evaluation of the upgraded 3-inch Hamamatsu photomultiplier for the KM3NeT neutrino telescope*, 2025 *JINST* **20** P07054.

[3] KM3NeT collaboration, *Observation of an ultra-high-energy cosmic neutrino with KM3NeT*, *Nature* **638** (2025) 376 [*Erratum ibid.* **640** (2025) E3] [INSPIRE].

[4] KM3NeT collaboration, *On the potential cosmogenic origin of the ultra-high-energy event KM3-230213A*, *Astrophys. J. Lett.* **984** (2025) L41 [arXiv:2502.08508] [INSPIRE].

[5] Pierre Auger collaboration, *The energy spectrum of cosmic rays beyond the turn-down around 10^{17} eV as measured with the surface detector of the Pierre Auger Observatory*, *Eur. Phys. J. C* **81** (2021) 966 [arXiv:2109.13400] [INSPIRE].

[6] Telescope Array collaboration, *The cosmic ray energy spectrum observed with the surface detector of the telescope array experiment*, *Astrophys. J. Lett.* **768** (2013) L1 [arXiv:1205.5067] [INSPIRE].

[7] KM3NeT collaboration, *On the potential galactic origin of the ultra-high-energy event KM3-230213A*, arXiv:2502.08387 [INSPIRE].

[8] KM3NeT et al. collaborations, *Characterizing candidate blazar counterparts of the ultra-high-energy event KM3-230213A*, arXiv:2502.08484 [INSPIRE].

[9] C.M. Urry and P. Padovani, *Unified schemes for radio-loud active galactic nuclei*, *Publ. Astron. Soc. Pac.* **107** (1995) 803 [astro-ph/9506063] [INSPIRE].

[10] P. Giommi and P. Padovani, *Astrophysical neutrinos and blazars*, *Universe* **7** (2021) 492 [arXiv:2112.06232] [INSPIRE].

[11] IceCube et al. collaborations, *Multimessenger observations of a flaring blazar coincident with high-energy neutrino IceCube-170922A*, *Science* **361** (2018) eaat1378 [arXiv:1807.08816] [INSPIRE].

[12] IceCube collaboration, *Evidence for neutrino emission from the nearby active galaxy NGC 1068*, *Science* **378** (2022) 538 [arXiv:2211.09972] [INSPIRE].

[13] ANTARES and OVRO collaborations, *Searches for neutrinos in the direction of radio-bright blazars with the ANTARES telescope*, *Astrophys. J.* **964** (2024) 3 [arXiv:2309.06874] [INSPIRE].

[14] X. Rodrigues et al., *The Spectra of IceCube Neutrino (SIN) candidate sources — V. Modeling and interpretation of multiwavelength and neutrino data*, *Astron. Astrophys.* **689** (2024) A147 [arXiv:2406.06667] [INSPIRE].

[15] M. Klinger et al., *AM^3: an open-source tool for time-dependent lepto-hadronic modeling of astrophysical sources*, *Astrophys. J. Suppl.* **275** (2024) 4 [arXiv:2312.13371] [INSPIRE].

[16] Fermi-LAT collaboration, *The spectrum of isotropic diffuse gamma-ray emission between 100 MeV and 820 GeV*, *Astrophys. J.* **799** (2015) 86 [arXiv:1410.3696] [INSPIRE].

[17] (IceCube Collaboration)§ and IceCube collaborations, *Search for extremely-high-energy neutrinos and first constraints on the ultrahigh-energy cosmic-ray proton fraction with IceCube*, *Phys. Rev. Lett.* **135** (2025) 031001 [arXiv:2502.01963] [INSPIRE].

[18] Pierre Auger collaboration, *Probing the origin of ultra-high-energy cosmic rays with neutrinos in the EeV energy range using the Pierre Auger Observatory*, *JCAP* **10** (2019) 022 [arXiv:1906.07422] [INSPIRE].

JCAP03(2026)033

[19] Pierre Auger collaboration, *Latest results from the searches for ultra-high-energy photons and neutrinos at the Pierre Auger Observatory*, *PoS* **ICRC2023** (2023) 1488 [INSPIRE].

[20] Pierre Auger collaboration, *Search for a diffuse flux of photons with energies above tens of PeV at the Pierre Auger Observatory*, *JCAP* **05** (2025) 061 [arXiv:2502.02381] [INSPIRE].

[21] X. Rodrigues et al., *Leptohadronic multi-messenger modeling of 324 gamma-ray blazars*, *Astron. Astrophys.* **681** (2024) A119 [arXiv:2307.13024] [INSPIRE].

[22] M. Ajello et al., *The origin of the extragalactic gamma-ray background and implications for dark-matter annihilation*, *Astrophys. J. Lett.* **800** (2015) L27 [arXiv:1501.05301] [INSPIRE].

[23] A. Palladino, X. Rodrigues, S. Gao and W. Winter, *Interpretation of the diffuse astrophysical neutrino flux in terms of the blazar sequence*, *Astrophys. J.* **871** (2019) 41 [arXiv:1806.04769] [INSPIRE].

[24] A. Dominguez et al., *Extragalactic background light inferred from AEGIS galaxy SED-type fractions*, *Mon. Not. Roy. Astron. Soc.* **410** (2011) 2556 [arXiv:1007.1459] [INSPIRE].

[25] KM3NeT collaboration, *Ultrahigh-energy event KM3-230213A within the global neutrino landscape*, *Phys. Rev. X* **15** (2025) 031016 [arXiv:2502.08173] [INSPIRE].

[26] A. Ambrosone et al., *Starburst galaxies strike back: a multi-messenger analysis with Fermi-LAT and IceCube data*, *Mon. Not. Roy. Astron. Soc.* **503** (2021) 4032 [arXiv:2011.02483] [INSPIRE].

[27] Fermi-LAT collaboration, *Resolving the extragalactic γ-ray background above 50 GeV with the Fermi Large Area Telescope*, *Phys. Rev. Lett.* **116** (2016) 151105 [arXiv:1511.00693] [INSPIRE].

[28] M. Lisanti, S. Mishra-Sharma, L. Necib and B.R. Safdi, *Deciphering contributions to the extragalactic gamma-ray background from 2 GeV to 2 TeV*, *Astrophys. J.* **832** (2016) 117 [arXiv:1606.04101] [INSPIRE].

[29] S.S. Wilks, *The large-sample distribution of the likelihood ratio for testing composite hypotheses*, *Annals Math. Statist.* **9** (1938) 60 [INSPIRE].

[30] IceCube collaboration, *Differential limit on the extremely-high-energy cosmic neutrino flux in the presence of astrophysical background from nine years of IceCube data*, *Phys. Rev. D* **98** (2018) 062003 [arXiv:1807.01820] [INSPIRE].

[31] IceCube collaboration, *The IceCube high-energy starting event sample: description and flux characterization with 7.5 years of data*, *Phys. Rev. D* **104** (2021) 022002 [arXiv:2011.03545] [INSPIRE].

[32] R. Abbasi et al., *Improved characterization of the astrophysical muon-neutrino flux with 9.5 years of IceCube data*, *Astrophys. J.* **928** (2022) 50 [arXiv:2111.10299] [INSPIRE].

[33] IceCube collaboration, *Detection of a particle shower at the Glashow resonance with IceCube*, *Nature* **591** (2021) 220 [*Erratum ibid.* **592** (2021) E11] [arXiv:2110.15051] [INSPIRE].

[34] ANTARES collaboration, *Constraints on the energy spectrum of the diffuse cosmic neutrino flux from the ANTARES neutrino telescope*, *JCAP* **08** (2024) 038 [arXiv:2407.00328] [INSPIRE].

[35] KM3Net collaboration, *Letter of intent for KM3NeT 2.0*, *J. Phys. G* **43** (2016) 084001 [arXiv:1601.07459] [INSPIRE].

JCAP03(2026)033

The KM3NeT collaboration

O. Adriani[b,a], A. Albert[c,be], A.R. Alhebsi[d], S. Alshalloudi[d], S. Alves Garre[e], A. Ambrosone[g,f,*], F. Ameli[h], M. Andre[i], L. Aphecetche[j], M. Ardid[k], S. Ardid[k], J. Aublin[l], F. Badaracco[n,m], L. Bailly-Salins[o], B. Baret[l], A. Bariego-Quintana[e], M. Barnard[p], Y. Becherini[l], M. Bendahman[f,*], F. Benfenati Gualandi[r,q], M. Benhassi[s,f], D.M. Benoit[t], Z. Beňušová[v,u], E. Berbee[w], C. van Bergen[w], E. Berti[b], V. Bertin[x], P. Betti[b], S. Biagi[y], M. Boettcher[p], D. Bonanno[y], M. Bondì[z], S. Bottai[b], A.B. Bouasla[bf], J. Boumaaza[aa], M. Bouta[x], M. Bouwhuis[w], C. Bozza[ab,f], R.M. Bozza[g,f], H. Brânzaş[ac], F. Bretaudeau[j], M. Breuhaus[x], R. Bruijn[ad,w], J. Brunner[x], R. Bruno[z], E. Buis[w], R. Buompane[s,f], I. Burriel[e], J. Busto[x], B. Caiffi[n], D. Calvo[e], A. Capone[h,ae], F. Carenini[r,q], V. Carretero[ad,w], T. Cartraud[l], P. Castaldi[af,q], V. Cecchini[e], S. Celli[h,ae], L. Cerisy[x], M. Chabab[ag], N. Chau[bg], A. Chen[ah], S. Cherubini[ai,y], T. Chiarusi[q], W. Chung[aj], M. Circella[ak], R. Clark[al], R. Cocimano[y], J.A.B. Coelho[l], A. Coleiro[l], A. Condorelli[l], R. Coniglione[y], P. Coyle[x], A. Creusot[l], G. Cuttone[y], R. Dallier[j], A. De Benedittis[s,f], X. de La Bernardie[j], G. De Wasseige[al], V. Decoene[j], P. Deguire[x], I. Del Rosso[r,q], L.S. Di Mauro[y], I. Di Palma[h,ae], A.F. Díaz[am], D. Diego-Tortosa[y], C. Distefano[y], A. Domi[an], C. Donzaud[l], D. Dornic[x], E. Drakopoulou[ao], D. Drouhin[c,be], J.-G. Ducoin[x], P. Duverne[l], R. Dvornický[v], T. Eberl[an], E. Eckerová[v,u], A. Eddymaoui[aa], T. van Eeden[w], M. Eff[l], D. van Eijk[w], I. El Bojaddaini[ap], S. El Hedri[l], S. El Mentawi[x], V. Ellajosyula[n], A. Enzenhöfer[x], M. Farino[aj], G. Ferrara[ai,y], M. D. Filipović[aq], F. Filippini[q], D. Franciotti[y], L.A. Fusco[ab,f], S. Gagliardini[ae,h], T. Gal[an], J. García Méndez[k], A. Garcia Soto[e], C. Gatius Oliver[w], N. Geißelbrecht[an], H. Ghaddari[ap], L. Gialanella[s,f], B.K. Gibson[t], E. Giorgio[y], I. Goos[l], P. Goswami[l], S.R. Gozzini[e], R. Gracia[an], B. Guillon[o], C. Haack[an], C. Hanna[aj], H. van Haren[ar], E. Hazelton[aj], A. Heijboer[w], L. Hennig[an], J.J. Hernández-Rey[e], A. Idrissi[y], W. Idrissi Ibnsalih[f], G. Illuminati[q], R. Jaimes[e], O. Janik[an], D. Joly[x], M. de Jong[as,w], P. de Jong[ad,w], B.J. Jung[w], P. Kalaczyński[bh,at], T. Kapoor[au], U.F. Katz[an], J. Keegans[t], V. Kikvadze[av], G. Kistauri[aw,av], C. Kopper[an], A. Kouchner[ax,l], Y. Y. Kovalev[ay], L. Krupa[u], V. Kueviakoe[w], V. Kulikovskiy[n], R. Kvatadze[aw], M. Labalme[o], R. Lahmann[an], M. Lamoureux[l], A. Langella[aj], G. Larosa[y], C. Lastoria[o], J. Lazar[al], A. Lazo[e], G. Lehaut[o], V. Lemaître[al], E. Leonora[z], N. Lessing[e], G. Levi[r,q], M. Lindsey Clark[l], F. Longhitano[z], A. Luashvili[p], S. Madarapu[e], F. Magnani[x], L. Malerba[n,m], F. Mamedov[u], A. Manfreda[f], A. Manousakis[az], M. Marconi[m,n], A. Margiotta[r,q], A. Marinelli[g,f], C. Markou[ao], L. Martin[j], M. Mastrodicasa[ae,h], S. Mastroianni[f], J. Mauro[al], K.C.K. Mehta[at], G. Miele[g,f], P. Migliozzi[f], E. Migneco[y], M.L. Mitsou[s,f], C.M. Mollo[f], L. Morales-Gallegos[s,f], N. Mori[b], A. Moussa[ap], I. Mozun Mateo[o], R. Muller[q], M.R. Musone[s,f], M. Musumeci[y], S. Navas[ba], A. Nayerhoda[ak], C.A. Nicolau[h], B. Nkosi[ah], B. Ó Fearraigh[n], V. Oliviero[g,f], A. Orlando[y], E. Oukacha[l], L. Pacini[a,b], D. Paesani[y], J. Palacios González[e], G. Papalashvili[ak,av], P. Papini[b], V. Parisi[m,n], A. Parmar[o], C. Pastore[ak], A. M. Păun[ac], G.E. Păvălaş[ac], S. Peña Martínez[l], M. Perrin-Terrin[x], V. Pestel[o], M. Petropavlova[u,bi], P. Piattelli[y], A. Plavin[ay,bj], C. Poirè[ab,f], V. Popa[ac,†], T. Pradier[c], J. Prado[e], S. Pulvirenti[y], C.A. Quiroz-Rangel[k], N. Randazzo[z], A. Ratnani[bb], S. Razzaque[bc], I.C. Rea[f], D. Real[e], G. Riccobene[y], J. Robinson[p], A. Romanov[o], E. Ros[ay], A. Šaina[e], F. Salesa Greus[e], D.F.E. Samtleben[as,w], A. Sánchez Losa[e], S. Sanfilippo[y], M. Sanguineti[m,n], D. Santonocito[y], P. Sapienza[y], M. Scaringella[b], M. Scarnera[al,l], J. Schnabel[an], J. Schumann[an], J. Seneca[w], M. Senniappan[d], P. A. Sevle Myhr[al], I. Sgura[ak], R. Shanidze[av],

JCAP03(2026)033

Chengyu Shao[bk,x], A. Sharma[l], Y. Shitov[u], F. Šimkovic[v], A. Simonelli[f], A. Sinopoulou[z], B. Spisso[f], M. Spurio[r,q], O. Starodubtsev[b], D. Stavropoulos[ao], I. Štekl[u], D. Stocco[j], M. Taiuti[m,n], Y. Tayalati[aa,bb], H. Thiersen[p], S. Thoudam[d], I. Tosta e Melo[z,ai], B. Trocmé[l], V. Tsourapis[ao], C. Tully[aj], E. Tzamariudaki[ao], A. Ukleja[at], A. Vacheret[o], V. Valsecchi[y], V. Van Elewyck[ax,l], G. Vannoye[m,n], E. Vannuccini[b], G. Vasileiadis[bd], F. Vazquez de Sola[w], A. Veutro[h,ae], S. Viola[y], D. Vivolo[s,f], A. van Vliet[d], E. de Wolf[ad,w], I. Lhenry-Yvon[l], S. Zavatarelli[n], D. Zito[y], J.D. Zornoza[e], J. Zúñiga[e]

[a] *Università di Firenze, Dipartimento di Fisica e Astronomia, via Sansone 1, Sesto Fiorentino, 50019 Italy*
[b] *INFN, Sezione di Firenze, via Sansone 1, Sesto Fiorentino, 50019 Italy*
[c] *Université de Strasbourg, CNRS, IPHC UMR 7178, F-67000 Strasbourg, France*
[d] *Khalifa University of Science and Technology, Department of Physics, PO Box 127788, Abu Dhabi, United Arab Emirates*
[e] *IFIC — Instituto de Física Corpuscular (CSIC — Universitat de València), c/Catedrático José Beltrán, 2, 46980 Paterna, Valencia, Spain*
[f] *INFN, Sezione di Napoli, Complesso Universitario di Monte S. Angelo, Via Cintia ed. G, Napoli, 80126 Italy*
[g] *Università di Napoli "Federico II", Dip. Scienze Fisiche "E. Pancini", Complesso Universitario di Monte S. Angelo, Via Cintia ed. G, Napoli, 80126 Italy*
[h] *INFN, Sezione di Roma, Piazzale Aldo Moro, 2 — c/o Dipartimento di Fisica, Edificio, G.Marconi, Roma, 00185 Italy*
[i] *Universitat Politècnica de Catalunya, Laboratori d'Aplicacions Bioacústiques, Centre Tecnològic de Vilanova i la Geltrú, Avda. Rambla Exposició, s/n, Vilanova i la Geltrú, 08800 Spain*
[j] *Subatech, IMT Atlantique, IN2P3-CNRS, Nantes Université, 4 rue Alfred Kastler — La Chantrerie, Nantes, BP 20722 44307 France*
[k] *Universitat Politècnica de València, Instituto de Investigación para la Gestión Integrada de las Zonas Costeras, C/ Paranimf, 1, Gandia, 46730 Spain*
[l] *Université Paris Cité, CNRS, Astroparticule et Cosmologie, F-75013 Paris, France*
[m] *Università di Genova, Via Dodecaneso 33, Genova, 16146 Italy*
[n] *INFN, Sezione di Genova, Via Dodecaneso 33, Genova, 16146 Italy*
[o] *LPC CAEN, Normandie Univ, ENSICAEN, UNICAEN, CNRS/IN2P3, 6 boulevard Maréchal Juin, Caen, 14050 France*
[p] *North-West University, Centre for Space Research, Private Bag X6001, Potchefstroom, 2520 South Africa*
[q] *INFN, Sezione di Bologna, v.le C. Berti-Pichat, 6/2, Bologna, 40127 Italy*
[r] *Università di Bologna, Dipartimento di Fisica e Astronomia, v.le C. Berti-Pichat, 6/2, Bologna, 40127 Italy*
[s] *Università degli Studi della Campania "Luigi Vanvitelli", Dipartimento di Matematica e Fisica, viale Lincoln 5, Caserta, 81100 Italy*
[t] *E.A. Milne Centre for Astrophysics, University of Hull, Hull, HU6 7RX, United Kingdom*
[u] *Czech Technical University in Prague, Institute of Experimental and Applied Physics, Husova 240/5, Prague, 110 00 Czech Republic*
[v] *Comenius University in Bratislava, Department of Nuclear Physics and Biophysics, Mlynska dolina F1, Bratislava, 842 48 Slovak Republic*
[w] *Nikhef, National Institute for Subatomic Physics, PO Box 41882, Amsterdam, 1009 DB Netherlands*
[x] *Aix Marseille Univ, CNRS/IN2P3, CPPM, Marseille, France*
[y] *INFN, Laboratori Nazionali del Sud, (LNS) Via S. Sofia 62, Catania, 95123 Italy*
[z] *INFN, Sezione di Catania, (INFN-CT) Via Santa Sofia 64, Catania, 95123 Italy*
[aa] *University Mohammed V in Rabat, Faculty of Sciences, 4 av. Ibn Battouta, B.P. 1014, R.P. 10000 Rabat, Morocco*
[ab] *Università di Salerno e INFN Gruppo Collegato di Salerno, Dipartimento di Fisica, Via Giovanni Paolo II 132, Fisciano, 84084 Italy*

JCAP03(2026)033

[ac] Institute of Space Science — INFLPR Subsidiary, 409 Atomistilor Street, Magurele, Ilfov, 077125 Romania
[ad] University of Amsterdam, Institute of Physics/IHEF, PO Box 94216, Amsterdam, 1090 GE Netherlands
[ae] Università La Sapienza, Dipartimento di Fisica, Piazzale Aldo Moro 2, Roma, 00185 Italy
[af] Università di Bologna, Dipartimento di Ingegneria dell'Energia Elettrica e dell'Informazione "Guglielmo Marconi", Via dell'Università 50, Cesena, 47521 Italia
[ag] Cadi Ayyad University, Physics Department, Faculty of Science Semlalia, Av. My Abdellah, P.O.B. 2390, Marrakech, 40000 Morocco
[ah] University of the Witwatersrand, School of Physics, Private Bag 3, Johannesburg, Wits 2050 South Africa
[ai] Università di Catania, Dipartimento di Fisica e Astronomia "Ettore Majorana", (INFN-CT) Via Santa Sofia 64, Catania, 95123 Italy
[aj] Princeton University, Department of Physics, Jadwin Hall, Princeton, New Jersey, 08544 U.S.A.
[ak] INFN, Sezione di Bari, via Orabona, 4, Bari, 70125 Italy
[al] UCLouvain, Centre for Cosmology, Particle Physics and Phenomenology, Chemin du Cyclotron, 2, Louvain-la-Neuve, 1348 Belgium
[am] University of Granada, Department of Computer Engineering, Automation and Robotics / CITIC, 18071 Granada, Spain
[an] Friedrich-Alexander-Universität Erlangen-Nürnberg (FAU), Erlangen Centre for Astroparticle Physics, Nikolaus-Fiebiger-Straße 2, 91058 Erlangen, Germany
[ao] NCSR Demokritos, Institute of Nuclear and Particle Physics, Ag. Paraskevi Attikis, Athens, 15310 Greece
[ap] University Mohammed I, Faculty of Sciences, BV Mohammed VI, B.P. 717, R.P. 60000 Oujda, Morocco
[aq] Western Sydney University, School of Science, Locked Bag 1797, Penrith, NSW 2751 Australia
[ar] NIOZ (Royal Netherlands Institute for Sea Research), PO Box 59, Den Burg, Texel, 1790 AB, the Netherlands
[as] Leiden University, Leiden Institute of Physics, PO Box 9504, Leiden, 2300 RA Netherlands
[at] AGH University of Krakow, Al. Mickiewicza 30, 30-059 Krakow, Poland
[au] LPC, Campus des Cézeaux 24, avenue des Landais BP 80026, Aubière Cedex, 63171 France
[av] Tbilisi State University, Department of Physics, 3, Chavchavadze Ave., Tbilisi, 0179 Georgia
[aw] The University of Georgia, Institute of Physics, Kostava str. 77, Tbilisi, 0171 Georgia
[ax] Institut Universitaire de France, 1 rue Descartes, Paris, 75005 France
[ay] Max-Planck-Institut für Radioastronomie, Auf dem Hügel 69, 53121 Bonn, Germany
[az] University of Sharjah, Sharjah Academy for Astronomy, Space Sciences, and Technology, University Campus — POB 27272, Sharjah, — United Arab Emirates
[ba] University of Granada, Dpto. de Física Teórica y del Cosmos & C.A.F.P.E., 18071 Granada, Spain
[bb] School of Applied and Engineering Physics, Mohammed VI Polytechnic University, Ben Guerir, 43150, Morocco
[bc] University of Johannesburg, Department Physics, PO Box 524, Auckland Park, 2006 South Africa
[bd] Laboratoire Univers et Particules de Montpellier, Place Eugène Bataillon — CC 72, Montpellier Cédex 05, 34095 France
[be] Université de Haute Alsace, rue des Frères Lumière, 68093 Mulhouse Cedex, France
[bf] Université Badji Mokhtar, Département de Physique, Faculté des Sciences, Laboratoire de Physique des Rayonnements, B. P. 12, Annaba, 23000 Algeria
[bg] Université Libre de Bruxelles, Science Faculty CP230, B-1050 Brussels, Belgium
[bh] AstroCeNT, Nicolaus Copernicus Astronomical Center, Polish Academy of Sciences, Rektorska 4, Warsaw, 00-614 Poland
[bi] Charles University, Faculty of Mathematics and Physics, Ovocný trh 5, Prague, 116 36 Czech Republic
[bj] Harvard University, Black Hole Initiative, 20 Garden Street, Cambridge, MA 02138 U.S.A.
[bk] School of Physics and Astronomy, Sun Yat-sen University, Zhuhai, China

[*] Corresponding author
[†] Deceased.

JCAP03(2026)033